Bidirectional changes in postmitotic H3K27me3 distributions underlie cerebellar granule neuron maturation dynamics

Vijyendra Ramesh[1,2], Fang Liu[1,3], Melyssa S. Minto[3], Urann Chan[3] and Anne E. West[2,3]

[1]These authors contributed equally

[2]Molecular Cancer Biology Program, Duke University School of Medicine, Durham, NC-27705

[3]Department of Neurobiology, Duke University School of Medicine, Durham, NC-27705

Abstract

The functional maturation of neurons is a prolonged process that extends beyond mitotic exit and requires the dynamic orchestration of gene transcription programs. We find that the postnatal maturation of cerebellar granule neurons (CGNs) is associated with dynamic changes in the genomic distribution of histone H3 lysine 27 trimethylation (H3K27me3), a chromatin modification best known for its role in cell fate specification. The developmental loss of H3K27me3 in postmitotic neurons is facilitated by the lysine demethylase KDM6B, and target genes induced in maturing CGNs show impaired expression with conditional KDM6B knockout. Interestingly, inhibition of the H3K27 methyltransferase EZH2 in newborn CGNs not only blocks the repression of progenitor genes but also impairs the induction of mature CGN genes, showing the importance of bidirectional regulation. These data demonstrate that H3K27me3 functions in developing postmitotic neurons to regulate the temporal coordination of gene expression programs that underlie functional neuronal maturation.

Introduction

Cell identity is determined during differentiation by the coordinated actions of chromatin regulatory factors, which serve to establish the accessibility of gene regulatory elements that control transcription of cell-type specific genes. Histone proteins play a key role in determining the architecture of chromatin, and specific post-translational modifications of the histones are tightly associated with the transcriptional state of a given locus or gene [1]. Among these modifications, histone methylation occurs on lysine and arginine residues of specific histones, and has roles in both gene activation and repression [2], and acts to alter gene transcription by recruiting the site-specific binding of effector proteins that carry out specialized functions [3]. The trimethylation of lysine 27 on histone H3 (H3K27me3) is a repressive histone modification that is best known for its role during cell-fate determination [4]. H3K27 methylation is deposited by the Polycomb repressive complex 2 (PRC2) lysine methyltransferases EZH1 and EZH2 [5, 6]. H3K27me3 can be enzymatically removed by the H3K27-specific lysine demethylases KDM6A (UTX) and KDM6B (JMJD3) [7]. In mice, null mutations in *Ezh2* result in early embryonic lethality [5], *Kdm6a* knockouts show severely impaired mid-gestational development [8], and *Kdm6b* knockouts die at birth [9] suggesting the physiological importance of H3K27me3 regulation for mammalian embryonic development.

At the cellular level, the functions of H3K27me3-dependent gene regulation in cell fate determination are well established [10]. In stem cells, the colocalization of H3K27me3 with the active histone marks H3K4me3 and H3K27ac at regulatory elements of cell-type specific genes is thought to poise these genes for subsequent activation or silencing upon terminal differentiation depending on the chosen fate of the cell. Activation of poised genes that function in the chosen fate is associated with the permanent loss of H3K27me3, whereas persistent silencing of genes that define alternative fates is mediated by recruitment of the PRC1 complex. However, the enzymes that regulate H3K27me3 remain expressed in fate-committed, postmitotic neurons both during postnatal stages of development and in the adult brain [11, 12], where their functions are less well understood. Genetic evidence that ongoing regulation of H3K27me3 after fate commitment might be important emerged when conditional

79 deletion of both *Ezh1* and *Ezh2* in neurons of the adult mouse striatum was shown to cause a
80 slow global loss of H3K27me3 as well as progressive neurodegeneration and death [13].
81 H3K27me3 may be required in terminally differentiated neurons to persistently repress genes
82 that have the potential to drive trans-differentiation to alternate cell fates. For example, in a
83 longitudinal study of postmitotic dopamine neurons undergoing directed differentiation in
84 culture, poised RNA Pol-II was found to colocalize with H3K27me3 at promoters of genes
85 encoding non-neuronal transcription factors (TFs) [14]. A separate study showed knockout of
86 the PRC2 component EED resulted in transcriptional de-repression of a set of TFs that have the
87 capacity to drive cellular reprogramming [13]. A non-exclusive possibility is that H3K27me3 is
88 required to maintain the expression of genes that define the terminal neuronal fate. Consistent
89 with this model, deleting EED in developing postmitotic dopamine or serotonin neurons *in vivo*
90 leads not only to loss of H3K27me3 but also to reduced expression of tyrosine hydroxylase (TH)
91 and tryptophan hydroxylase 2 (TPH2), respectively, which, as the key enzymes that mediate
92 dopamine and serotonin synthesis, define the transmitter phenotype of these
93 neuromodulatory neurons [15].
94
95 These data suggest that dynamic changes in H3K27me3 in postmitotic neurons could
96 play a role in plasticity of cell fate or function and raise the question of the molecular
97 mechanisms that can control this distribution. The global depletion of H3K27me3 in neurons
98 takes months to appear after deletion of EZH1/2 [13] revealing that this histone modification is
99 remarkably stable across the bulk of the genome. Furthermore, whereas histone replacement is
100 a major mechanism of H3K27me3 removal in dividing cells [16], histone turnover is very slow in
101 postmitotic neurons [17]. Instead, lysine demethylases may have a privileged role in the local
102 regulation of histone methylation patterns in postmitotic neurons [18]. Both *Kdm6a* and *Kdm6b*
103 are expressed in neurons over the course of brain development, though only *Kdm6b* shows
104 enhanced expression following exposure of cells to neuronal differentiation cues [12, 19-21].
105 Germline knockout of *Kdm6b* does not impair the gross architecture of the embryonic brain,
106 but it does result in perinatal lethality caused by disruption of respiratory circuit maturation [9].
107 To identify functions of histone H3K27 demethylation in postmitotic stages of

108 neurodevelopment, we previously conditionally deleted *Kdm6a* and *Kdm6b* in *Atoh1*-expressing
109 cerebellar granule neuron (CGN) progenitors of the mouse. We used CGNs to model
110 neurodevelopment because they comprise more than 99% of all neurons [22] and 85% of cells
111 [23] in the cerebellum, enabling the *in vivo* comparison of chromatin across CGN
112 developmental states with limited contamination from other cell types. When purified and
113 placed in *ex vivo* culture, CGN progenitors coordinately exit the cell cycle, minimizing
114 heterogeneity of cell developmental stage across the population [24]. In both preparations,
115 gene transcription programs change over time coincident with changes in CGN biology (*e.g.,*
116 proliferation, migration, synapse formation, synapse maturation [25, 26]). Loss of *Kdm6a/b* had
117 no effect on postnatal morphogenesis of the cerebellum, demonstrating these enzymes are not
118 required *in vivo* for regulation of CGN progenitor proliferation. However knockdown of *Kdm6b*
119 in cultured CGNs impaired the developmental induction of genes during the period of
120 postmitotic neuronal maturation [12]. Based on these data, we hypothesized that H3K27me3
121 may serve as a temporal gatekeeper of these maturation genes, delaying their activation
122 beyond the immediate period of terminal differentiation to the neuronal fate.
123
124 Here we investigated the contribution of H3K27me3 dynamics to changing programs of
125 gene transcription in maturing CGNs. We used ChIP-seq and CUT&RUN to identify the genomic
126 location and timing of differential sites of H3K27me3 enrichment across the genome of CGNs
127 developing *in vivo* and in culture. We observed that H3K27me3 distributions continue to
128 change even after fate committed CGN progenitors exit the cell cycle, and that the loss of
129 H3K27me3 at gene promoters is associated with the activation of genes induced as neurons
130 mature. We used both genetic and pharmacological approaches to disrupt the action of
131 H3K27me3 regulatory enzymes and show evidence of roles for both the lysine demethylase
132 KDM6B and the lysine methyltransferase EZH2 in the induction of a postmitotic program of
133 gene transcription that underlies functional maturation of CGNs. Taken together, our data
134 advance understanding of how programs of gene expression are temporally orchestrated in
135 maturing neurons.
136

137 # Materials and Methods

138

139 **Animal Husbandry**

140 We performed all procedures under an approved protocol from the Duke University Institutional
141 Animal Care and Use Committee. *Kdm6b* floxed mice described in [27] were obtained from
142 Jackson Labs (Stock #029615, RRID #IMSR_JAX:029615). These mice contain *loxP* sites flanking
143 exon 14-20, encoding the catalytic Jumonji-C domain, of the mouse *Kdm6b* gene on chromosome
144 11. *Atoh1-cre* mice were obtained from Jackson Labs (Stock #011104, RRID #IMSR_JAX:011104).
145 Mice were genotyped by ear clipping at the time of weaning using protocols described on the
146 Jackson Labs website. CD-1 IGS mice (#Strain 022, #IMSR_CRL:022) and C57BL/6NCrl mice
147 (#Strain 027, RRID #IMSR_CRL:027) were obtained from Charles River Laboratories. Both male
148 and female mice were used for all experiments in this study.

149

150 **CGN Culture**

151 Cerebella of CD1-IGS mice were dissected at P6-P8. Cells were dissociated and run on a Percoll
152 gradient to isolate cerebellar granule neuron progenitors (GNPs) as previously described [28].
153 GNPs were plated at a density of 1 million cells/well in a 24-well plate for RNA or protein isolation.
154 At day *in vitro* 2 (DIV2) CGNs were treated with 1 µM Cytosine Arabinoside (AraC) (Sigma #C1768)
155 to block division of any non-neuronal cells. KDM6 and EZH2 inhibitors were added at the doses
156 and days described in the text.

157

158 **RT-qPCR**

159 CGNs were lysed in TRIzol Reagent (Thermo #15596026) at a volume of 0.25 mL per 1 million cells
160 for RNA purification. Isolated RNA was analyzed using a nanodrop to determine concentration
161 and purity, after which it was treated with DNase I (NEB #M0303S). We made Oligo(dT) primed
162 cDNA using SuperscriptII Reverse Transcriptase (Invitrogen #19064014). qPCR was carried out on
163 an Applied Biosystems Quantstudio 3 Thermal cycler using Power SYBR Green PCR Master Mix
164 (Thermo #4367659) and PCR primers targeting the gene/locus of interest (**Supplementary**
165 **Information, Table S1)**.

166

167 **RNA-seq**

168 RNA for RNA-seq was obtained by processing cerebellar tissue or CGN cultures with Trizol reagent
169 followed by clean up on the Zymo Direct-zol RNA miniprep kit (Zymo #R2052). RNA purity was
170 measured to ensure samples had A260/280 and A260/230 values > 1.9. RNA was then polyA
171 enriched and 150 bp paired-end sequencing was performed by Novogene, Inc on an Illumina Hi-
172 seq 2000 machine.

173

174 **Chromatin Immunoprecipitation**

175 **Cerebellar Tissue:** We pooled cerebellum from three C57BL/6NCrl (Charles River Laboratories
176 IMSR Cat# CRL:027, RRID: IMSR_CRL:027) P7 mice, two P14 mice and one P60 mouse for each
177 biological replicate. Both male and female mice were used. Cerebellum samples were dounced
178 in a glass homogenizer containing 2 ml of 1% formaldehyde (w/v) PBS buffer per sample and
179 kept at 25 °C for 15 min, washed twice with cold PBS, lysed in 600 µl lysis buffer (1% SDS (w/v),
180 10 mM EDTA, and 50 mM Tris, pH 8.1). The cross-linked material was sonicated with a
181 Bioruptor (Diagenode), with output set to "high" with 30 s on/off cycles to an average size
182 range of 150–350 bp which was then determined by agarose gel electrophoresis. Sonicated
183 chromatin was centrifuged for 10 minutes at 14000 RPM at 4°C, after which the supernatant
184 was diluted 10-fold in dilution buffer (0.01% SDS, 1.1% Triton X-100, 1.2 mM EDTA, 16.7 mM
185 Tris-HCl, pH 8.1, 167 mM NaCl). Prior to immunoprecipitation, 6 µl of antibody (anti-H3K27Me3,
186 Active Motif 39155, RRID: AB_2561020) was incubated with 100 µl of Dynabeads Protein G
187 (Invitrogen 10004D) in PBS for 4-6h at 4 °C. The antibody-bead conjugate was then washed
188 twice with cold PBS, and added to 6 ml of cell lysis for overnight immunoprecipitation at 4˚C.
189 The following day, bead-bound DNA-protein complexes were washed, eluted, and purified
190 using a PCR purification kit (Cat# 28104, Qiagen). ChIP-seq libraries were made using the
191 MicroPlex Library Preparation kit V2 (C05010012, Diagenode); and 50 bp single-end sequencing
192 was performed at the Duke Sequencing and Analysis Core Resource on a Hi-Seq 2000 machine.
193 Three independent biological replicates were performed for each antibody and developmental
194 time point and ChIP reagents were prepared according to the Millipore 17–295 ChIP kit.

195

196 **Nuclear Isolation of CGNs for CUT&RUN**

197 CGNs were scraped into 1X DPBS at 0.25 mL per 1 million cells and then 'pop-spun' according to
198 the REAP method [29], until the rotor reached 7000 rpm. Pellets were then washed once with 1X
199 DPBS and pop-spun again, after which they were resuspended in Nuclei Isolation Buffer (20 mM
200 HEPES pH 7.9, 10 mM KCl, 2 mM Spermidine, 0.1% v/v Triton X-100, 20% v/v glycerol), incubated
201 on ice for 5 minutes and then spun at 2,000g for 5 min at 4˚C. After this step the supernatant was
202 removed, and pelleted nuclei were then resuspended in Nuclei Storage Buffer (20 mM Tris-HCl
203 pH 8.0, 75 mM NaCl, 0.5 mM EDTA, 50% v/v glycerol, 1 mM DTT, 0.1 mM PMSF) and stored in -
204 80˚C until ready to process.

205

206 **CUT&RUN**

207 CUT&RUN was performed on nuclei isolated from CGN cultures using the CUTANA
208 ChIC/CUT&RUN kit (EpiCypher #14-1408) as per manufacturer guidelines. Specific changes made
209 to the protocol are noted here. Nuclei in Nuclei Storage Buffer were pelleted and resuspended in
210 Nuclei Isolation Buffer. Nuclei were then incubated with activated ConA beads. Antibodies used
211 for CUT&RUN were: H3K27me3 (Active Motif 39155, RRID: AB_2561020), H3K4me3 and IgG
212 (positive and negative controls included in kit). CUT&RUN libraries were made using the NEB
213 Ultra II DNA Library Prep Kit for Illumina (NEB #E7645L), and NEBNext Multiplex Oligos for
214 Illumina (96 Unique Dual Index Primer Pairs) (NEB #E6440S). Library cleanup was performed prior
215 to and after PCR amplification using 0.8X Kapa Hyperpure beads (Roche #08963851001). PCR
216 amplification was performed with the following parameters as described in the EpiCypher
217 CUT&RUN kit: 1) 98˚C, 45 sec; 2) 98˚C, 15 sec; 60˚C, 10 sec x 14 cycles; 3) 72˚C, 60 sec. Libraries
218 were then pooled and 50 bp paired-end sequencing was performed at the Duke Sequencing and
219 Analysis Core Resource on a NovaSeq 6000 S-Prime flow cell.

220

221 **Sequencing Data Analysis**

222 **ChIP-seq:**

223 ChIP-seq reads were quality scored and screened through fastQC, trimmed for adapter
224 sequences using Trimmomatic 0.38 and then aligned to the mouse GRCm38.p4 reference
225 genome using STAR 2.7.2b. Alignments were filtered for mapped reads using samtools and then
226 normalized using the bamCoverage function of the deepTools2.0 suite. ChIP-seq tracks were
227 generated using bamCoverage, to generate continuous BigWig files. Peak calling was performed
228 using Macs2, with parameters for broad peaks and an FDR threshold of 0.01. The R package
229 DESeq2 [30] was used for read-count normalization and differential binding analysis. R package
230 ChIPseeker [31] was used to annotate ChIP-seq peaks using a window of TSS $\pm$ 3000.
231 'Promoters' is a group of ChIPseeker terms 'Promoter (<=1kb), Promoter (1-2 kb) and Promoter
232 (2-3 kb). Gene Body is a group of terms 5' UTR, 3' UTR, Intron and Exon.
233
234 **CUT&RUN:**
235 CUT&RUN reads were processed the same as ChIP-seq reads until peak-calling. Peak calling was
236 performed using Macs2, with parameters for broad peaks and an FDR threshold of 0.1.
237 Metagene plots were created using SeqPlots [32], by inputting bigwig and BED files and setting
238 a window of TSS +/- 5000 bp.
239
240 **RNA-seq**
241 RNA-seq reads were processed similarly to ChIP-seq reads until and excluding peak calling. Read
242 counts for genes were generated using HTseq2 count, with feature type set to 'exon', and the
243 Gencode GRCm38.p4 GTF annotation file. DESeq2 was used for read-count normalization and
244 differential expression analysis.
245
246 **Data Processing**
247 Heatmaps were generated using the Broad Institute's Morpheus tool:
248 https://software.broadinstitute.org/Morpheus, with the following clustering parameters:
249 hierarchical clustering, complete linkage, one minus spearman rank correlation, cluster by rows.
250 VST-transformed counts used to generate heatmaps and clusters are provided in Table S2. Gene

251 ontology analysis was performed using the GO consortium GO tool [33, 34] using terms related
252 to 'biological process'.
253
254 **Western Blot**
255 **Cerebellar Tissue:** For preparation of protein lysates from cerebellar tissue, we pooled
256 cerebellum from two P7 mice, one P14 and one P60 mouse for each biological replicate.
257 Cerebellum samples were dounced 50 times with PBS in glass homogenizer, centrifuged at 8000
258 x g for 5 minutes, and washed twice by cold PBS, then pellets were re-suspended in 300 µL
259 extraction buffer (10 mM HEPES, pH 7.9, 1.5 mM $MgCl_2$, 10 mM KCl), supplemented with 1X
260 protease inhibitor cocktail (Roche, Indianapolis, IN). Thereafter, 60µL of 1N HCl was added to
261 the cell lysates and kept on ice for 30 minutes, following which the cell lysates were centrifuged
262 at 11,000 x g for 10 minutes at 4 ºC. Protein concentration of acid-soluble supernatants was
263 measured using Pierce BCA protein assay kit (Cat # 23227, Thermo). 20 µg of acid-soluble
264 supernatant was used for western blots. Samples were loaded onto wells of a 10-20% gradient
265 gel and run at 150V for 30-40 min in running buffer (25 mM Tris-HCl, 192 mM Glycine, 0.1% w/v
266 SDS) after which protein was transferred onto a PVDF membrane (BioRad #1620177) in transfer
267 buffer (25 mM Tris-HCl, 192 mM Glycine, 20% v/v Methanol) for 1 hour at 100V or overnight at
268 30V. The membrane was blocked for 1 hour in 5% (w/v) BSA (Sigma #A3059) in TBST. After the
269 blocking step, the membrane was incubated with primary antibody overnight at 4˚C. The
270 following day, primary antibody was removed, after which the membranes were washed three
271 times with TBST for 5 minutes each, incubated with secondary antibody for 1 hour, and then
272 again washed three times with TBST for 5 minutes each. At the end of this, membranes were
273 imaged using the Li-Cor Odyssey using appropriate exposure times for the target antibodies.
274
275 **CGN Culture**: Cells were scraped into PBS from 6 well plates at the relevant endpoints,
276 centrifuged at 200 x g for 5 minutes, and washed twice with PBS. Pellets were then
277 resuspended in 100 µL of extraction buffer (described above), after which 20 µL of 1N HCl was
278 added. Samples were hereafter processed as described above.
279

280 **Antibodies:** The antibodies used were H3K27Ac (Abcam ab4729), H3K27Me3 (Active Motif
281 39155, RRID: AB_2561020), and Total H3 (Tissue: Millipore 05-499, Culture: Cell Signaling 9715).
282 Western blot signals were detected by Li-Cor Odyssey InfraRed Imaging System (Lincoln, NE)
283 with the secondary antibodies, CF770 goat anti-Rabbit, (Biotium 20078) and CF 680 goat anti-
284 mouse, (Biotium 20065). Protein bands were quantified using ImageJ.
285
286 **GEO Accession Codes**
287 H3K27me3 ChIP-seq data for P7, P14 and P60 cerebellum, WT and *Kdm6b*-cKO cerebellum;
288 RNA-seq data for WT and *Kdm6b*-cKO cerebellum; CUT&RUN and RNA-seq data for cultured
289 CGNs can be accessed at GEO: GSE212441. RNA-seq data for P7, P14 and P60 cerebellum and
290 DIV0 and DIV7 CGNs, H3K27ac, ZIC1/2 ChIP-seq data and DHS-seq data for P7 and P60
291 cerebellum were adapted from Frank et. al 2015 [26].
292
293 **Author Contributions**
294 Conceptualization: V.R., F.L. and A.E.W.; Methodology: V.R., F.L., U.C., and A.E.W.; Formal
295 Analysis: V.R., M.M.; Investigation V.R.; Resources, A.E.W.; Writing: V.R., A.E.W.; Funding
296 Acquisition: A.E.W.
297
298 **Acknowledgements**
299 Fig schematics in Fig 1A, 3A and 5A were created using biorender.com. This work was
300 supported by NIH grant R01NS0988804.

301 # Results

302
303 Cerebellar Maturation Involves Dynamic, Genome-Wide Changes in H3K27me3 Distribution
304 To measure H3K27me3 dynamics during cerebellar maturation, we harvested cerebellar
305 cortex from C57BL/6NCrl mice at postnatal days 7, 14, and 60 (Fig. 1A). At P7, about half of all
306 cells in the mouse cerebellum are proliferating granule neuron precursors (GNPs) whereas the
307 rest are immature, postmitotic cerebellar granule neurons (CGNs). By P14 GNP cell division has

308 ceased, and the cerebellum is composed of immature postmitotic CGNs that are migrating to the
309 inner granule layer (IGL) where they receive synapses and fully mature by P60 [23, 26]. Western
310 blot of acid extracted histones showed a significant global increase in total H3K27me3 levels from
311 P7 to P14 that was maintained at P60 (Fig 1B), whereas total H3K27ac fell in a similar temporal
312 pattern (Fig. S1A). These data are consistent with the PRC2-dependent restriction of cell potential
313 upon terminal differentiation [4].
314
315 However, when we assessed the genomic location of H3K27me3 by ChIP-seq (Fig S1B) we
316 observed a more complex pattern. We found local losses as well as gains in H3K27me3
317 enrichment at different sites between developmental stages (Fig 1C). This was true even when
318 comparing P14 with P60 (Fig 1C), demonstrating that bidirectional changes in H3K27me3
319 distributions occur during postmitotic stages of neuronal maturation, well after the period of
320 terminal cell fate commitment has ended (Fig S1C). We stratified differential H3K27me3 ChIP-
321 seq peaks by their genomic location with respect to proximal gene promoters, gene bodies or
322 intergenic regions (Fig 1D), and found a consistent overrepresentation of proximal gene
323 promoters among developmentally demethylated peaks for all three comparisons. By contrast,
324 H3K27me3 ChIP-seq peaks differentially gained between all three comparisons did not differ
325 from the global distribution of H3K27me3, which was distributed across gene-body and distal
326 intergenic regions as well as proximal promoters. The percentage of total H3K27me3-positive
327 promoters gradually decreased by ~2-fold from P7 to P60, while that of H3K27me3-positive distal
328 intergenic regions increased, and that of gene bodies stayed about the same over time (Fig 1E).
329 Additionally, the total number of H3K27me3 peaks called centered within a 5 kb window around
330 the TSS appeared to gradually decrease from P7 to P60 (Fig 1E). These data demonstrate that in
331 CGNs H3K27me3 patterns are locally regulated in postmitotic neurons, suggesting a function for
332 H3K27me3-dependent gene regulation in developing neurons that extends beyond the
333 restriction of cell fate commitment.
334
335 <u>H3K27me3 Dynamics at Promoters During Cerebellar Maturation Inversely Correlate with Gene</u>
336 <u>Expression</u>

337 We filtered differential H3K27me3-peaks for those occurring at promoters because these
338 regions can be directly mapped to their likely target gene for transcriptional regulation. We then
339 asked whether peaks that were up- and downregulated over stages of CGN differentiation were
340 found at genes that can be stratified according to cellular function. Examples of genes with
341 promoter-associated peaks lost or gained from P7 to P60, respectively, were the genes encoding
342 the mature NMDA-type glutamate receptor *Grin2c* which is strongly expressed in mature CGNs
343 [12] and the cell-proliferation factor *Mycn,* which is expressed only in GNPs [35] (Fig 1F). This is
344 consistent with the hypothesis that changes in the levels of promoter H3K27me3 inversely
345 correlate with changes in gene expression over development.
346
347 To determine if the correlation of H3K27me3 demethylation with transcriptional
348 maturation held more broadly, we first performed hierarchical clustering on all differential
349 H3K27me3 ChIP-seq peaks and identified 3 major clusters with differing direction and timing of
350 change (Fig 2A). The first cluster, which we termed 'H3K27me3 Up,' contained peaks that gained
351 methylation as early as P14 and maintained methylation during CGN maturation. Gene Ontology
352 (GO) analysis demonstrated that these peaks were enriched for genes associated with progenitor
353 functional terms related to cell proliferation and morphogenesis. The next two clusters included
354 demethylated peaks, that we termed 'H3K27me3 Down (Fast)' and 'H3K27me3 Down (Slow)'
355 respectively, depending on whether they changed between P7 and P14 or between P14 and P60.
356 Both clusters were enriched for neuronal GO terms. Because developmentally gained peaks
357 showed a broader distribution than just promoters, we also performed the same type of filtering
358 and hierarchical clustering for differential H3K27me3 peaks overlying gene bodies (Fig S2). This
359 resulted in three clusters, two of which contained peaks that gained and lost methylation
360 respectively at gene-bodies. Both these clusters were enriched for neuronal GO terms including
361 early CGN-maturation genes. Together, these data show that bidirectional H3K27me3 dynamics
362 are distinct across distinct genomic locations.
363
364 We then asked if H3K27me3 dynamics at gene promoters were associated with the
365 expression of the corresponding RNA transcript across CGN maturation (Fig 2B, C). For this

366 purpose, we compared our H3K27me3 ChIP-seq to a dataset of gene expression at the same time
367 points from our previous study [26]. We found that 'H3K27me3 Up' peaks at gene promoters
368 were significantly associated with a decrease in expression of the associated gene over the same
369 period of developmental time and 'H3K27me3 Down' peaks were associated with an increase in
370 gene expression. Among the H3K27me3 Down peaks, 'Fast' peaks were associated with a
371 significantly greater magnitude of gene induction than 'Slow' peaks between P7 and P14, but
372 'Slow' peaks were associated with a significantly greater magnitude of gene induction than 'Fast'
373 peaks between P14 and P60. There was no significant difference between 'Fast' and 'Slow' peaks
374 from P7 to P60 indicating that it is the timing not the magnitude of differential developmental
375 gene expression that defines the two clusters. These data show that the kinetics of H3K27me3
376 demethylation at gene promoters are associated with the timing of gene expression changes in
377 postmitotic neurons, which allows for multiple postmitotic waves of gene expression (Fig. 2C).
378
379 <u>*Kdm6b*-cKO Impairs CGN Maturation via Promoter Hypermethylation</u>
380 The developmental loss of H3K27me3 at a subset of gene promoters in CGNs could occur
381 through changes in expression of the enzymes that maintain or remove these histone
382 modifications. At the level of gene expression, RNA-seq counts of the H3K27 methyltransferases
383 *Ezh1/2* and the H3K27 demethylases *Kdm6a*/b showed that although there was a developmental
384 switch between the dominant reader and writer enzymes, the overall expression levels of each
385 class of enzyme did not change over time (Fig S3). However, previous *in situs* from our lab
386 demonstrated that *Kdm6b* expression is transiently induced in newborn CGNs in the inner EGL,
387 and we further showed that shRNA-mediated knockdown of *Kdm6b* in cultured CGNs impairs the
388 expression of a subset of developmentally induced genes [12]. Thus, we considered the
389 possibility that KDM6B might mediate postmitotic loss of H3K27me3 at a subset of
390 developmentally induced gene promoters in the developing cerebellum *in vivo* to promote their
391 transcriptional induction. To test this hypothesis, we conditionally knocked out *Kdm6b* in
392 cerebellar granule neuron precursor cells (GNPs) *in vivo* by crossing heterozygous transgenic
393 *Atoh1-Cre* mice with *Kdm6b*$^{fl/fl}$ mice. We then harvested cerebellar tissue from littermates that
394 were either *Kdm6b*$^{fl/fl}$ (WT) or *Atoh1-Cre; Kdm6b*$^{fl/fl}$ (*Kdm6b*-cKO) at P14 as an intermediate

395 developmental time point for CGN maturation [26] (Fig 3A). We processed this tissue to perform
396 either RNA-seq (Fig S4A) or ChIP-seq for H3K27me3 (Fig S4B). We used DESeq2 to compute
397 differentially enriched H3K27me3 ChIP peaks between WT and *Kdm6b*-cKO tissue at P14, and
398 obtained 250 upregulated peaks, and 327 downregulated peaks (FDR < 0.05, |Log2FC| > 1) (Fig
399 3B). We then mapped these differential peaks to their genomic location (Fig 3C). We found peaks
400 with elevated levels of H3K27me3 in *Kdm6b*-cKO mice to be significantly more likely to be within
401 gene promoters compared with the overall distribution of peaks or the distribution of peaks that
402 had reduced H3K27me3 in *Kdm6b*-cKO mice. We observed that the percentage of promoter
403 associated H3K27me3 peaks decreased between WT and *Kdm6b*-cKO mice, while peaks in distal
404 intergenic regions and gene-bodies increased (Fig S5C). The genes containing promoters with
405 increased H3K27me3 in the *Kdm6b*-cKO were enriched for neuronal GO terms (Fig 3D), whereas
406 those containing promoters with decreased H3K27me3 in the *Kdm6b*-cKO mice failed to pull any
407 significant GO terms. Overall, these observations mirror our findings of H3K27 demethylation at
408 the promoters of neuronal maturation genes and suggests that KDM6B mediates that process.
409
410 To determine the relationship between H3K27me3 levels at promoters and gene
411 expression in the *Kdm6b*-cKO mice, we computed the correlation between *Kdm6b*-cKO
412 associated differential H3K27me3 enrichment at promoter regions, with the expression of the
413 associated gene in WT and *Kdm6b*-cKO mice. These data showed that the gain of H3K27me3 is
414 associated with a significant loss of gene expression (Fig 3E) as exemplified by the synaptic genes
415 *Grm4* and *Gabbr2* (Fig 3F). By contrast, promoters that lost H3K27me3 in *Kdm6b*-cKO mice
416 showed no significant difference in gene expression (Fig 3E). These data suggest that
417 developmental loss of H3K27me3 at the promoters of genes induced in CGNs during postmitotic
418 maturation is facilitated by KDM6B, and that this loss promotes the developmental induction of
419 gene expression.
420
421 <u>H3K27me3 Removal at CGN-Maturation Gene Promoters is Associated with H3K27ac Enrichment</u>
422 <u>and Increased Chromatin Accessibility</u>

423 Previously we showed CGN maturation to occur in concert with broad, genome-wide
424 changes in H3K27ac [26] (Fig S5A). To ask whether H3K27me3 removal at promoters overlapped
425 with the gain of H3K27ac, we computed the overlap between genes containing promoter peaks
426 that were H3K27ac Up (|L2FC| > 0, FDR < 0.05) and H3K27me3 Down (Fig S5B). We observed that
427 only a subset of genes that gained H3K27ac also lost H3K27me3 at P60. H3K27ac Up genes that
428 were H3K27me3 Down (912 genes), or not H3K27me3 Down (4208 genes) were both highly
429 enriched for neuronal GO terms (Fig S5C).
430
431 To determine what characterizes the subset of promoters that become demethylated we
432 sought to ask what transcription factors might be found at these gene promoters compared to
433 all H3K27me3-positive promoters. To conduct an unbiased screen, we first utilized the tool called
434 Binding Analysis for Regulation of Transcription (BART) [36], which calculates enrichments of
435 previously published ChIP-seq TF binding profiles within a defined set of genomic regions. We
436 first filtered our ChIP-seq data for genes associated with the 'H3K27me3-Down' peak cluster
437 described in Fig 2A, combining 'Down (Fast)', and 'Down (Slow)' clusters, and obtained predicted
438 transcription factors (TF) whose binding significantly overlaps these gene promoters. We
439 compared the enrichment statistics of TFs enriched in these clusters to those derived from all
440 H3K27me3– promoter associated genes (Fig 4A). As expected, we found PRC2 components EZH2,
441 JARID2, SUZ12 to be significantly enriched across both the H3K27me3-Down cluster and all
442 H3K27me3-promoter associated genes. However, we found only the H3K27me3-Down cluster to
443 be significantly enriched for the putative binding of transcription factors ZIC1 and ZIC2, which
444 previous work from our group has shown to be a driver of CGN maturation [26]. Importantly,
445 when we assessed the 'H3K27me3-Down (Fast)', and 'H3K27me3-Down (Slow)' clusters
446 separately (Fig S6A), they were also enriched for the binding of ZIC1 and ZIC2, which is consistent
447 with evidence [26] that these TFs function at multiple stages of CGN differentiation. By contrast,
448 when we performed the same analysis for the 'H3K27me3-Up' cluster (Fig S6A), we found this
449 set of promoters was significantly enriched for the binding of a distinct set of TFs involved in cell
450 differentiation, namely SOX3, FOXF1, SHOX2, POU3F2 as well as histone deacetylation (HDAC1)
451 [37].

452 To directly compare changes in ZIC1/2 TF binding to changes in H3K27me3 across CGN
453 development, we re-analyzed our previously published ZIC1/2 ChIP-seq data [26] and measured
454 ZIC1/2 binding at All Genes, Genes with H3K27me3 Up, and Genes with H3K27me3 Down (Fig
455 4A). We then identified gene promoters with increased ZIC binding at P60 compared with P7. We
456 termed these genes 'ZIC Up' and first compared them to the H3K27me3-Down cluster. We found
457 that 56% of H3K27me3-Down genes were also ZIC-Up, and that these genes were enriched for
458 neuronal GO terms (Fig 4B). As a control, we compared 'ZIC Up' genes to H3K27me3-Up genes
459 (Fig. S6A) and only found an overlap of only 11%. We repeated this analysis with the H3K27me3
460 ChIP-seq peaks that were differential at P14 between WT and *Kdm6b*-cKO (Fig. 3) and found a
461 similar enrichment of putative ZIC1 and ZIC2 binding within gene promoters associated with
462 H3K27me3 peaks 'Up in *Kdm6b*-cKO' (Fig S6B), but not 'Down in *Kdm6b*-cKO' (Fig S6C). 72% of
463 the 'H3K27me3 Up in *Kdm6b*-cKO' genes were also 'ZIC Up' (Fig S6B) and were enriched for
464 neuronal GO terms. Only 9% of 'H3K27me3 Down in *Kdm6b*-cKO' were also 'ZIC Up' (Fig S6C). As
465 examples of gene promoters that belong to both the H3K27me3-Down cluster, and H3K27me3
466 Up peaks due to *Kdm6b*-cKO, we show tracks for *Grin2c* and *Grm4,* that are strongly enriched for
467 ZIC1/2 at their promoters at P60 (Fig 4C).
468
469 We have shown previously [26] that increased ZIC1/2 binding strongly correlates with the
470 developmental enrichment of H3K27ac and increased chromatin accessibility during cerebellar
471 maturation. Given the strong enrichment of ZIC1/2 binding within the H3K27me3-Down cluster
472 during development, and H3K27me3 Up peaks due to *Kdm6b*-cKO, we wanted to ask whether
473 H3K27me3 turnover during cerebellar maturation is associated with H3K27ac enrichment and
474 changes in chromatin accessibility. As such we computed the distribution of Log2FC values from
475 our previously published H3K27ac-ChIP-seq and DNAse Hypersensitivity data [26] comparing P7
476 and P60 cerebellum and filtered these distributions for those related to peaks belonging to our
477 differential H3K27me3 promoter clusters. Indeed, H3K27me3 Down peaks at P60 were
478 significantly associated with an increase in H3K27ac enrichment (Fig 4D) and DNAse
479 hypersensitivity (Fig 4E). H3K27me3-Up peaks due to *Kdm6b*-cKO conversely were associated
480 with genes that became enriched with H3K27ac, and DNAse hypersensitive regions at P60 (Fig

481 S6D). As examples, we show H3K27ac ChIP-seq and DNAse-seq tracks for 'H3K27me3 Down' gene
482 *Grin2c*, and 'H3K27me3 Up' gene *Atoh1*. Thus, these data provide further evidence that the
483 postmitotic removal of H3K27me3 from a subset of gene promoters is important for the
484 coordinated induction of gene expression that underlies neuronal maturation.
485
486 Modulation of H3K27me3 Turnover Mediates CGN Maturation Gene-Regulation in Culture
487 To determine the functional consequences of modulating H3K27me3 at CGN-maturation
488 gene promoters or gene bodies we used cultures of primary mouse CGNs as context for
489 pharmacological manipulation of histone regulatory enzymes. When GNPs isolated from P6-8
490 mouse cerebellum are placed in culture they show changes in gene expression over the course
491 of 7 days [26] (Fig 5A, S7A, B). We performed CUT&RUN-seq to measure genome-wide changes
492 in H3K27me3 after 1, 3, 5 and 7 days *in vitro* (DIV) (Fig 5A). We found methylation to be gained
493 quickly after cell cycle exit, with 1688 peaks significantly up between DIV1 and DIV3 CGNs,
494 followed by 109 peaks between DIV3 and DIV5, and 2 peaks between DIV5 and DIV7 CGNs (Fig
495 5B). Like our observations *in vivo* (Fig 1, 2), we saw that demethylation occurred more gradually,
496 with 477 peaks significantly down between DIV1 and DIV3 CGNs, followed by 227 and 25 peaks
497 between DIV3 and DIV5, and DIV5 and DIV7 CGNs respectively. Again, consistent with our
498 findings *in vivo*, we found demethylation to occur primarily at promoters (Fig 5C, Fig S7C), and
499 gains in methylation to occur more uniformly, including at gene-bodies and distal intergenic
500 regions. When we filtered for differential H3K27me3 peaks at gene promoters, they clustered in
501 two groups that gain H3K27me3 or lose H3K27me3 at DIV7 (Fig 5D). Genes whose promoters
502 were in the 'Gain H3K27me3 at DIV7' cluster were associated with cell fate specification GO terms
503 as predicted by canonical PRC functions. Conversely, genes whose promoters were in the 'Lose
504 H3K27me3 at DIV7' cluster were associated with functional neuronal GO terms. We observed
505 mature synaptic genes such as *Grin2c* and *Grm4* to lose H3K27me3 from DIV1 to DIV7 (Fig 5E
506 lower), and proliferation genes expressed in GNPs such as *Myc* and *Atoh1* to gain H3K27me3
507 from DIV1 to DIV7 in culture (Fig 5E upper). Finally, we stratified our previously published RNA-
508 seq data between DIV0 and DIV7 CGNs by their respective methylation status ('Gain H3K27me3
509 at DIV7' or 'Lose H3K27me3 at DIV7' cluster) and calculated the distribution of Log2FC (Fig 5F).

510 We found peaks associated with the 'Gain H3K27me3 at DIV7' cluster to have a significant
511 reduction in gene expression over time in culture, and those associated with the 'Lose H3K27me3
512 at DIV7' cluster to have a significant gain in gene expression by DIV7 (Fig 5F, S7D, E). These data
513 show that we can use this CGN culture system to explore mechanisms and causality with respect
514 to the enzymes mediating H3K27me3 turnover and gene regulation during CGN maturation.
515
516 To determine the functional contribution of H3K27me3 regulation to CGN-maturation
517 gene expression, we treated CGN cultures at DIV1 with small molecule inhibitors of either EZH2
518 or KDM6A/B, called GSK-126 and GSK-J4 respectively, and measured the consequences for cell
519 viability, histone modification, and gene expression at DIV5. Because these drugs have not been
520 widely used in primary neurons, we first performed a cell viability assay and measured the IC_{50}
521 values of both drugs. We determined the IC_{50} values to be ~3.07 µM for GSK-J4 and ~7.32 µM for
522 GSK-126, respectively (Fig S8A). For the KDM6B inhibitor, the IC_{50} was nearly 10-fold below the
523 dose (25 µM) used in the original characterization studies to block the histone demethylase
524 activity of these enzymes [38]. Thus, we sought to determine if these drugs could block enzymatic
525 function in viable cells. Choosing concentrations below the measured IC_{50} values, we first
526 measured global levels of H3K27me3 by western blot (Fig 6A), after treating with 0, 0.5, 1.0 and
527 2.0 µM of either drug. Treatment of CGNs with GSK-126 caused a dose-dependent loss of
528 H3K27me3 validating the method. GSK-126 treatment also appeared to cause a global increase
529 (Fig S8B) in H3K27ac, which is consistent with the idea that H3K27me3 and H3K27ac are mutually
530 exclusive modifications that oppose each other's functions [39]. By contrast, GSK-J4 treatment
531 failed to cause any dose-dependent change in H3K27me3 or H23K27ac detected by western.
532
533 Given our evidence that KDM6B facilitates demethylation of a subset of gene promoters
534 over development (Fig 2), even in the absence of global reductions in H3K27me3 (Fig 1), we asked
535 whether there might be local changes in H3K27me3 after GSK-J4 treatment. We treated CGNs
536 daily with 1 µM of GSK-J4 between DIV1-DIV5 and then assessed H3K27me3 peaks across the
537 genome by CUT&RUN-seq to determine if there were local increases in H3K27me3 at a subset of
538 genes (Fig S7C-D). We failed to observe any significant changes in H3K27me3 enrichment across

539 the genome at this concentration of GSK-J4 (Fig S8E), with biological replicate being the primary
540 factor for variation in this dataset (Fig S8D). We did find 1µM GSK-J4 treatment to slightly
541 decrease mRNA levels of specific neuronal function genes (Fig S8F), suggesting that the drug may
542 act to regulate genes in a demethylation independent manner in CGNs. We conclude that the
543 therapeutic range of GSK-J4 is too small in our CGNs cultures to permit its use for inhibition of
544 KDM6-dependent demethylation.
545
546 Our data showed that EZH2-inhibiting doses of GSK-126 were compatible with CGN
547 viability, thus we then used CUT&RUN-seq for H3K27me3 on CGNs treated with 5 µM GSK-126
548 (Fig 6B, Fig S9A). Most of the regions that showed differential methylation following GSK-126
549 treatment had lower levels of H3K27me3 in GSK-126 treated neurons, consistent with the
550 inhibition of this histone methyltransferase (Fig 6B). A much smaller number of peaks showed
551 increases in H3K27me3, which may arise from secondary effects of EZH2 inhibition on other
552 processes that impact H3K27me3 distributions such as EZH1 function [40] or histone turnover
553 [41]. Regions that lost H3K27me3 after GSK-126 treatment showed a similar genomic distribution
554 to the overall distribution of H3K27me3 peaks in CGNs (Fig 9B-C). Demethylated peaks were
555 enriched for GO terms associated with several non-neuronal cell types, consistent with the
556 general hypothesis that PRC functions in postmitotic cells at least in part to maintain the chosen
557 cell fate [14] (Fig S9D).
558
559 To determine how EZH2 activity influences H3K27me3 distribution at early genes, we
560 created metagene plots (Fig 6C) describing H3K27me3 coverage across all H3K27me3 peaks
561 compared with the differential peaks from Fig 5D. We observed GSK-126 treatment to
562 significantly reduce H3K27me3 coverage across the 'Gain H3K27me3 at DIV7' cluster but not the
563 'Lose H3K27me3 at DIV7' cluster or at all H3K27me3 peaks. To determine the effects of GSK-126
564 treatment on gene expression, we performed RNA-seq and identified 259 significantly
565 downregulated and 393 significantly upregulated genes (Fig 6D, (upper)). Upregulated genes
566 included *Mycn*, *Ebf3* and *Jag1* and were enriched for GO terms including 'regulation of cell
567 proliferation', while downregulated genes included *Gabrd*, *Gabra6*, *Grm4* and were enriched for

568 synaptic GO terms (Fig 6D, (lower)). We then computed gene expression profiles of CGNs
569 maturing in culture (from DIV0 to DIV7) to CGNs treated with GSK-126 (Fig 6 left). We found
570 genes repressed due to GSK-126 treatment to be strongly induced at DIV7 compared to DIV0.
571 Conversely, we saw genes upregulated at DIV0 such as *Mycn* and *Ebf3* to be induced upon GSK-
572 126 treatment. Furthermore, we computed changes to gene expression in response to GSK-126
573 treatment as a function of clusters described in Fig 5E – 'All peaks', 'Gain H3K27me3 at DIV7' and
574 'Lose H3K27me3 at DIV7' (Fig 6E right). We observed GSK-126 treatment to significantly
575 upregulate the expression of genes belonging to the 'Gain H3K27me3 at DIV7' cluster, and
576 significantly downregulate the expression of genes belonging to the 'Lose H3K27me3 at DIV7'
577 cluster (Fig 6D, (upper right)). Visualizing H3K27me3 and RNA-seq tracks at early gene *Ebf3*, we
578 observed GSK-126 treatment to completely block H3K27me3 and induce gene expression
579 compared to DMSO treatment (Fig 6F upper). The late synaptic gene *Gabrd*, conversely,
580 remained unchanged with respect to H3K27me3 enrichment, but was strongly downregulated in
581 response to GSK-126 treatment (Fig 6F lower). These data show that EZH2 functions in newly
582 postmitotic neurons to add H3K27me3 to genes that were not methylated at the time of cell fate
583 commitment, and that this methylation helps to repress expression of progenitor genes [42] in
584 neurons. By contrast, EZH2 is not required over this time course for the maintenance of
585 H3K27me3 at genes that possessed the modification at the time of terminal differentiation,
586 consistent with the slow turnover of methylated histones in postmitotic neurons. Why EZH2
587 catalytic activity early on during CGN maturation is critical for the induction of late genes is a
588 point we discuss below.

589

590 ## Discussion

591

592 In this study, we investigated the role of H3K27me3 turnover in postmitotic gene
593 regulation, using the maturation of mouse CGNs as a model system. PRC2 activity has long been
594 studied as a mechanism of early cell-fate specification in mammals through the deposition of
595 H3K27me3 and silencing of fate defining genes during the differentiation of embryonic stem cells

596 (ESCs) into other cell types including neural progenitor cells (NPCs) and early neurogenesis [5, 43,
597 44]. Our study demonstrates that dynamic changes in H3K27me3 continue in postmitotic
598 neurons at specific sites in the genome to coordinate the temporal induction of gene expression
599 programs that underlie functional maturation. Increases in H3K27me3 occurred rapidly after cell
600 cycle exit, whereas promoter demethylation occurred gradually and these turnover kinetics
601 strongly correlated with the kinetics of induced gene expression. Promoters and gene bodies that
602 gained H3K27me3 after cell cycle exit were enriched for genes involved in proliferation and cell-
603 fate specification such as *Atoh1* and *Myc*. By contrast, developmentally demethylated promoters
604 included those for genes that confer mature function on synapses such as the NMDA receptor
605 subunit *Grin2c* and the metabotropic glutamate receptor *Grm4*. This suggested to us that there
606 are temporally coordinated mechanisms of enzymatic H3K27me3 turnover during CGN
607 maturation, and that postmitotic H3K27me3 demethylation may be a key step for timing
608 functional synaptic maturation.
609
610 Our *in vivo* cerebellar data show that developmental loss of H3K27me3 from gene
611 promoters is facilitated by the H3K27me3 demethylase KDM6B, and further that conditional
612 knockout of KDM6B in CGNs impaired the expression of genes that are induced as CGNs mature.
613 *Kdm6b* expression is upregulated in newborn CGNs in the inner EGL [12], and we speculate that
614 the temporal increase in expression of this enzyme may tip the balance of H3K27me3 regulation
615 to favor histone demethylation at specific target sites. Our evidence that genes with increased
616 H3K27me3 in the *Kdm6b*-cKO mice overlap those that show developmental loss of H3K27me3 is
617 consistent with the possibility that KDM6B functions enzymatically to demethylate histones at
618 these gene promoters. However, chromatin regulators including KDM6B have scaffolding
619 functions as well as enzymatic functions [45-49], thus we attempted to use pharmacological
620 inhibition of KDM6B to validate the role of its enzymatic activity in developing CGN gene
621 regulation. The small molecule GSK-J4 is a highly selective inhibitor of the KDM6 family compared
622 with other histone demethylases, and it was previously demonstrated in primary human
623 macrophages to block LPS-mediated histone demethylation and induction of TNFα expression
624 with an IC_{50} of 9 μM and no apparent toxicity up to 30 μM [38]. By contrast we found 50%

625 cytotoxicity in CGNs at a GSK-J4 concentration of just 3.1 µM and no evidence by western blot or
626 CUT&RUN for any global or local changes in H3K27me3 when the drug was applied at the non-
627 toxic dose of 1 µM. Moving forward, as an alternative to pharmacological inhibition of KDM6B,
628 genetic mutation of the JmjC domain of KDM6B may be a more effective means to test its
629 functional requirement in neuronal H3K27me3 demethylation [50]. Indeed, a prior study showed
630 that in a BAC transgene, enzymatically dead KDM6B was unable to rescue perinatal death in
631 KDM6B knockout mice, which is consistent with a requirement for the enzymatic function of
632 KDM6B in maturation of the respiratory circuit [9].
633
634 Our observation that H3K27me3 removal occurs at only a subset of genes that are
635 developmentally induced during CGN maturation raises the question of how these promoters are
636 marked for methylation and demethylation. Through an unbiased approach, we showed that
637 promoters that lose H3K27me3 during CGN maturation are strongly enriched for binding of the
638 transcription factors ZIC1/2; thus, one possibility is that an interaction between KDM6B and the
639 ZICs selects these genes for induction in maturing neurons. ZIC1/2 are strong drivers of CGN
640 maturation [26], and mutation of these genes is associated with cerebellar disorders, showing
641 their importance in CGN development [51, 52]. ZIC1 and 2 are zinc-finger binding proteins that
642 exhibit dynamic DNA binding properties during cerebellar maturation, and they regulate the
643 expression of both early and late CGN maturation genes [26]. Given the strong association of
644 H3K27ac enrichment at these promoters, however, it is likely that ZIC1/2 binding is a
645 consequence and not a cause of H3K27-demethylation at promoters. It would therefore be
646 essential to measure the genome-wide enrichment patterns of KDM6B during CGN maturation,
647 in order to identify its binding partners and direct targets. Existing literature investigating KDM6B
648 dynamics across the epigenome is sparse owing to the lack of well validated, commercially
649 available KDM6B antibodies. Nevertheless, KDM6B has been shown to localize to promoters and
650 enhancers of neurogenic genes in NSCs [53, 54], and more recently to induce muscle
651 regeneration gene *Has2*, by removing H3K27me3 from its promoter, to initiate muscle repair in
652 response to injury [50]. KDM6B targeting to these specific loci might be facilitated through
653 interactions with TFs [54, 55], and chromatin remodeling complexes [56]. For example, KDM6B

654 has been shown to strongly associate with the ATP-dependent chromatin remodeler mSWI/SNF
655 or BAF complex, by interacting with its subunits which in turn potentiate its activity [57]. This
656 interaction has been shown to play a role in neuronal development [57, 58].

657 Interestingly, we find that maturation of CGN transcriptional programs not only depends
658 on the loss of H3K27me3 at genes that turn on late, but also requires the addition of H3K27me3
659 at regions that gain this mark in newly postmitotic neurons. Using CUT&RUN in cultured CGNs,
660 we discovered that the rapid increases in H3K27me3 that accumulate in newly postmitotic
661 neurons are highly sensitive to inhibition of EZH2 with GSK-126. Failure to gain H3K27me3 at
662 these sites in differentiating neurons not only prevented the developmental downregulation of
663 CGN progenitor markers like *Mycn* and *Ebf3* but also impaired the developmental induction of
664 late genes like *Gabrd*, *Grm4* and *Grin2c*. The impact of GSK-126 on the mature CGN
665 transcriptional program was not due to changes in H3K27me3 regulation at the late genes
666 themselves. This shows that the postmitotic addition of H3K27me3 at specific genomic sites is
667 crucial in regulating the induction of genes that turn on well after neuronal cell fate is
668 determined. However, these data also raise the question of how PRC2 complex function can
669 indirectly regulate the activation of late gene expression programs over a period of days. One
670 possibility is that the persistent expression of early TFs like MYCN and EBF3 interferes with the
671 expression or function of the TFs that activate late gene promoters even once these promoters
672 lose H3K27me3. However, another possibility may be via the effects of H3K27me3 on chromatin
673 architecture. Though H3K27me3 is an acutely repressive mark, PRC2 dependent deposition of
674 H3K27me3 has been shown in some cases to contribute to physical interactions between
675 enhancers and their target genes by anchoring chromatin loops [59, 60]. These loops may then
676 poise genes for enhancer activation later upon receiving a developmental stimulus. The gain of
677 H3K27me3 in early differentiating CGNs could serve a similar function to establish such enhancer
678 contacts with the promoters of late genes such that when KDM6B demethylates these
679 promoters, the enhancer can permit activation. In the future, investigating dynamics in higher-
680 order chromatin structure through low-input techniques such as HiCAR [61] might help inform
681 how H3K27me3 dynamics contribute to gene regulation in postmitotic neurons.
682

683 References

684

685 1. Hyun, K., et al., *Writing, erasing and reading histone lysine methylations.* Experimental &
686 Molecular Medicine, 2017. **49**(4): p. e324-e324.
687 2. Jambhekar, A., A. Dhall, and Y. Shi, *Roles and regulation of histone methylation in animal*
688 *development.* Nature Reviews Molecular Cell Biology, 2019. **20**(10): p. 625-641.
689 3. Daniel, J.A., M.G. Pray-Grant, and P.A. Grant, *Effector proteins for methylated histones:*
690 *an expanding family.* Cell Cycle, 2005. **4**(7): p. 919-26.
691 4. van Mierlo, G., et al., *The Complexity of PRC2 Subcomplexes.* Trends in Cell Biology, 2019.
692 **29**(8): p. 660-671.
693 5. O'Carroll, D., et al., *The polycomb-group gene Ezh2 is required for early mouse*
694 *development.* Mol Cell Biol, 2001. **21**(13): p. 4330-6.
695 6. Voncken, J.W., et al., *Rnf2 (Ring1b)*
696 *deficiency causes gastrulation arrest and cell cycle inhibition.* Proceedings of the National
697 Academy of Sciences, 2003. **100**(5): p. 2468.
698 7. Swigut, T. and J. Wysocka, *H3K27 Demethylases, at Long Last.* Cell, 2007. **131**(1): p. 29-
699 32.
700 8. Welstead, G.G., et al., *X-linked H3K27me3 demethylase Utx is required for embryonic*
701 *development in a sex-specific manner.* Proc Natl Acad Sci U S A, 2012. **109**(32): p. 13004-
702 9.
703 9. Burgold, T., et al., *The H3K27 demethylase JMJD3 is required for maintenance of the*
704 *embryonic respiratory neuronal network, neonatal breathing, and survival.* Cell Rep, 2012.
705 **2**(5): p. 1244-58.
706 10. Margueron, R. and D. Reinberg, *The Polycomb complex PRC2 and its mark in life.* Nature,
707 2011. **469**(7330): p. 343-9.
708 11. Wijayatunge, R., et al., *The histone lysine demethylase Kdm6b is required for activity-*
709 *dependent preconditioning of hippocampal neuronal survival.* Mol Cell Neurosci, 2014. **61**:
710 p. 187-200.
711 12. Wijayatunge, R., et al., *The histone demethylase Kdm6b regulates a mature gene*
712 *expression program in differentiating cerebellar granule neurons.* Molecular and Cellular
713 Neuroscience, 2018. **87**: p. 4-17.
714 13. von Schimmelmann, M., et al., *Polycomb repressive complex 2 (PRC2) silences genes*
715 *responsible for neurodegeneration.* Nature Neuroscience, 2016. **19**(10): p. 1321-1330.
716 14. Ferrai, C., et al., *RNA polymerase II primes Polycomb-repressed developmental genes*
717 *throughout terminal neuronal differentiation.* Molecular Systems Biology, 2017. **13**(10):
718 p. 946.
719 15. Toskas, K., et al., *PRC2-mediated repression is essential to maintain identity and function*
720 *of differentiated dopaminergic and serotonergic neurons.* Science Advances. **8**(34): p.
721 eabo1543.
722 16. Shpargel, K.B., et al., *KDM6 demethylase independent loss of histone H3 lysine 27*
723 *trimethylation during early embryonic development.* PLoS Genet, 2014. **10**(8): p.
724 e1004507.

725 17. Maze, I., et al., *Critical Role of Histone Turnover in Neuronal Transcription and Plasticity.*
726 Neuron, 2015. **87**(1): p. 77-94.
727 18. Swahari, V. and A.E. West, *Histone demethylases in neuronal differentiation, plasticity,*
728 *and disease.* Curr Opin Neurobiol, 2019. **59**: p. 9-15.
729 19. Jepsen, K., et al., *SMRT-mediated repression of an H3K27 demethylase in progression from*
730 *neural stem cell to neuron.* Nature, 2007. **450**(7168): p. 415-9.
731 20. Burgold, T., et al., *The histone H3 lysine 27-specific demethylase Jmjd3 is required for*
732 *neural commitment.* PLoS One, 2008. **3**(8): p. e3034.
733 21. De Santa, F., et al., *Jmjd3 contributes to the control of gene expression in LPS-activated*
734 *macrophages.* Embo j, 2009. **28**(21): p. 3341-52.
735 22. Consalez, G.G., et al., *Origins, Development, and Compartmentation of the Granule Cells*
736 *of the Cerebellum.* Frontiers in Neural Circuits, 2021. **14**: p. 88.
737 23. Altman, J., *Development of the Cerebellar System.* Relation to its Evolution, Structure, and
738 Functions., 1997.
739 24. Fogarty, M.P., et al., *Fibroblast growth factor blocks Sonic hedgehog signaling in neuronal*
740 *precursors and tumor cells.* Proceedings of the National Academy of Sciences, 2007.
741 **104**(8): p. 2973-2978.
742 25. Sathyanesan, A., et al., *Emerging connections between cerebellar development, behaviour*
743 *and complex brain disorders.* Nature Reviews Neuroscience, 2019. **20**(5): p. 298-313.
744 26. Frank, C.L., et al., *Regulation of chromatin accessibility and Zic binding at enhancers in the*
745 *developing cerebellum.* Nature Neuroscience, 2015. **18**(5): p. 647-656.
746 27. Manna, S., et al., *Histone H3 Lysine 27 demethylases Jmjd3 and Utx are required for T-cell*
747 *differentiation.* Nat Commun, 2015. **6**: p. 8152.
748 28. Bilimoria, P.M. and A. Bonni, *Cultures of cerebellar granule neurons.* CSH Protoc, 2008.
749 **2008**: p. pdb.prot5107.
750 29. Suzuki, K., et al., *REAP: A two minute cell fractionation method.* BMC Research Notes,
751 2010. **3**(1): p. 294.
752 30. Love, M.I., W. Huber, and S. Anders, *Moderated estimation of fold change and dispersion*
753 *for RNA-seq data with DESeq2.* Genome Biology, 2014. **15**(12): p. 550.
754 31. Yu, G., L.-G. Wang, and Q.-Y. He, *ChIPseeker: an R/Bioconductor package for ChIP peak*
755 *annotation, comparison and visualization.* Bioinformatics, 2015. **31**(14): p. 2382-2383.
756 32. Stempor, P. and J. Ahringer, *SeqPlots - Interactive software for exploratory data analyses,*
757 *pattern discovery and visualization in genomics [version 1; peer review: 2 approved, 1*
758 *approved with reservations].* Wellcome Open Research, 2016. **1**(14).
759 33. Ashburner, M., et al., *Gene ontology: tool for the unification of biology. The Gene Ontology*
760 *Consortium.* Nat Genet, 2000. **25**(1): p. 25-9.
761 34. *The Gene Ontology resource: enriching a GOld mine.* Nucleic Acids Res, 2021. **49**(D1): p.
762 D325-d334.
763 35. Ma, M., et al., *N-myc is a key switch regulating the proliferation cycle of postnatal*
764 *cerebellar granule cell progenitors.* Scientific Reports, 2015. **5**(1): p. 12740.
765 36. Wang, Z., et al., *BART: a transcription factor prediction tool with query gene sets or*
766 *epigenomic profiles.* Bioinformatics, 2018. **34**(16): p. 2867-2869.

767 37. Wang, T.-W., et al., *Sox3 expression identifies neural progenitors in persistent neonatal*
768 *and adult mouse forebrain germinative zones.* Journal of Comparative Neurology, 2006.
769 **497**(1): p. 88-100.
770 38. Kruidenier, L., et al., *A selective jumonji H3K27 demethylase inhibitor modulates the*
771 *proinflammatory macrophage response.* Nature, 2012. **488**(7411): p. 404-408.
772 39. Lavarone, E., C.M. Barbieri, and D. Pasini, *Dissecting the role of H3K27 acetylation and*
773 *methylation in PRC2 mediated control of cellular identity.* Nature Communications, 2019.
774 **10**(1): p. 1679.
775 40. Shen, X., et al., *EZH1 mediates methylation on histone H3 lysine 27 and complements EZH2*
776 *in maintaining stem cell identity and executing pluripotency.* Mol Cell, 2008. **32**(4): p. 491-
777 502.
778 41. Chory, E.J., et al., *Nucleosome Turnover Regulates Histone Methylation Patterns over the*
779 *Genome.* Mol Cell, 2019. **73**(1): p. 61-72.e3.
780 42. Consalez, G.G., et al., *Origins, Development, and Compartmentation of the Granule Cells*
781 *of the Cerebellum.* Front Neural Circuits, 2020. **14**: p. 611841.
782 43. Mohn, F., et al., *Lineage-Specific Polycomb Targets and De Novo DNA Methylation Define*
783 *Restriction and Potential of Neuronal Progenitors.* Molecular Cell, 2008. **30**(6): p. 755-766.
784 44. Pereira, J.D., et al., *Ezh2, the histone methyltransferase of PRC2, regulates the balance*
785 *between self-renewal and differentiation in the cerebral cortex.* Proceedings of the
786 National Academy of Sciences, 2010. **107**(36): p. 15957-15962.
787 45. Kim, E., et al., *Phosphorylation of EZH2 activates STAT3 signaling via STAT3 methylation*
788 *and promotes tumorigenicity of glioblastoma stem-like cells.* Cancer Cell, 2013. **23**(6): p.
789 839-52.
790 46. Kim, J., et al., *Polycomb- and Methylation-Independent Roles of EZH2 as a Transcription*
791 *Activator.* Cell Rep, 2018. **25**(10): p. 2808-2820.e4.
792 47. Miller, S.A., S.E. Mohn, and A.S. Weinmann, *Jmjd3 and UTX play a demethylase-*
793 *independent role in chromatin remodeling to regulate T-box family member-dependent*
794 *gene expression.* Mol Cell, 2010. **40**(4): p. 594-605.
795 48. Xun, J., et al., *JMJD3 suppresses stem cell-like characteristics in breast cancer cells by*
796 *downregulation of Oct4 independently of its demethylase activity.* Oncotarget, 2017.
797 **8**(13): p. 21918-21929.
798 49. Ohguchi, H., et al., *KDM6B modulates MAPK pathway mediating multiple myeloma cell*
799 *growth and survival.* Leukemia, 2017. **31**(12): p. 2661-2669.
800 50. Nakka, K., et al., *JMJD3 activated hyaluronan synthesis drives muscle regeneration in an*
801 *inflammatory environment.* Science, 2022. **377**(6606): p. 666-669.
802 51. Twigg, S.R., et al., *Gain-of-Function Mutations in ZIC1 Are Associated with Coronal*
803 *Craniosynostosis and Learning Disability.* Am J Hum Genet, 2015. **97**(3): p. 378-88.
804 52. Blank, M.C., et al., *Multiple developmental programs are altered by loss of Zic1 and Zic4*
805 *to cause Dandy-Walker malformation cerebellar pathogenesis.* Development, 2011.
806 **138**(6): p. 1207-16.
807 53. Park, Dae H., et al., *Activation of Neuronal Gene Expression by the JMJD3 Demethylase Is*
808 *Required for Postnatal and Adult Brain Neurogenesis.* Cell Reports, 2014. **8**(5): p. 1290-
809 1299.

54. Estarás, C., et al., *Genome-wide analysis reveals that Smad3 and JMJD3 HDM co-activate the neural developmental program.* Development, 2012. **139**(15): p. 2681-2691.
55. Dai, J.P., et al., *Jmjd3 activates Mash1 gene in RA-induced neuronal differentiation of P19 cells.* J Cell Biochem, 2010. **110**(6): p. 1457-63.
56. De Santa, F., et al., *The Histone H3 Lysine-27 Demethylase Jmjd3 Links Inflammation to Inhibition of Polycomb-Mediated Gene Silencing.* Cell, 2007. **130**(6): p. 1083-1094.
57. Narayanan, R., et al., *Loss of BAF (mSWI/SNF) Complexes Causes Global Transcriptional and Chromatin State Changes in Forebrain Development.* Cell Reports, 2015. **13**(9): p. 1842-1854.
58. Nguyen, H., et al., *Epigenetic Regulation by BAF Complexes Limits Neural Stem Cell Proliferation by Suppressing Wnt Signaling in Late Embryonic Development.* Stem Cell Reports, 2018. **10**(6): p. 1734-1750.
59. Cruz-Molina, S., et al., *PRC2 Facilitates the Regulatory Topology Required for Poised Enhancer Function during Pluripotent Stem Cell Differentiation.* Cell Stem Cell, 2017. **20**(5): p. 689-705.e9.
60. Kraft, K., et al., *Polycomb-mediated genome architecture enables long-range spreading of H3K27 methylation.* Proceedings of the National Academy of Sciences, 2022. **119**(22): p. e2201883119.
61. Wei, X., et al., *HiCAR is a robust and sensitive method to analyze open-chromatin-associated genome organization.* Molecular Cell, 2022. **82**(6): p. 1225-1238.e6.

Figures and Captions

Fig 1. The maturing mouse cerebellum undergoes a genome-wide redistribution of H3K27me3 dominated by loss at promoters

A) CD1 mice were sacrificed at postnatal days 7, 14 and 60 after which cerebellar tissue was dissected out and processed to harvest histones, chromatin and RNA. B) (Left) Western blot of acid extracted histone from cerebellar tissue for H3K27me3 and total Histone H3 (n=3 biological replicates), (Right) Quantification of Western Blot, one-way ANOVA, * indicates $p < 0.05$. C) MA plot showing H3K27me3 peaks gained (Up) and lost (Down) throughout cerebellar maturation *in vivo* (n=3 biological replicates, differential enrichment calculated using DESeq2 package. Up and Down are loci with FDR < 0.05 and |L2FC| > 1). D) Percentage of differential H3K27me3 peaks between P7-P14, P14-P60 and P7-P60, annotated by genomic region (Annotation performed using ChIPseeker package, TSS +/- 3000 bp). E) (Left) Percentage of H3K27me3 peaks annotated by genomic region, (Right) Heatmap of H3K27me3 peaks centered around TSS +/- 5000 *bp*. F)

845 ChIP-seq tracks of example 'Down' gene *Grin2c* (Upper) and 'Up' gene *Myc* (lower) (y-axes for
846 ChIP-seq tracks are autoscaled according to data range in current view).
847
848 **Fig 2. Differentially methylated promoters cluster by turnover kinetics and correlate with CGN**
849 **maturation gene expression**
850 A) (Left) Heatmap of hierarchically clustered, VST-transformed DESeq2-normalized counts of
851 differential H3K27me3 promoter peaks from P7-P60, (Right) Corresponding Gene Ontology (GO)
852 Terms associated with nearest gene and FDR. B) Violin plot showing the distribution of Log2FC of
853 gene expression as a function of clustering performed in A, across developmental time (one-way
854 ANOVA, * indicates $p < 0.05$). C) Example ChIP-seq tracks of genomic loci belonging to clusters
855 described in A, at *Mycn*, *Grm4* and *Grin2c* loci and corresponding RNA-seq tracks (y-axes for ChIP-
856 seq and RNA-seq tracks are autoscaled separately, according to data range in current view).
857
858 **Fig 3. *Kdm6b* knockout in CGN precursors impairs CGN maturation via H3K27me3**
859 **hypermethylation of CGN maturation gene promoters**
860 A) *Atoh1-Cre*; *Kdm6b*$^{fl/fl}$ (cKO) and *Kdm6b*$^{fl/fl}$ (WT) mice were generated by crossing *Atoh1-Cre*;
861 *Kdm6b*$^{fl/+}$ mice to *Kdm6b*$^{fl/fl}$ mice and sacrificed at P14 for cerebellar tissue harvest and
862 subsequent performing of H3K27me3 ChIP-seq (WT n=2, cKO n=3 biological replicates) and RNA-
863 seq (n=2 biological replicates). B) MA plot showing differential enrichment of genome wide
864 H3K27me3 peaks between WT and cKO mice ($|Log2FC| > 1$, $FDR < 0.05$). C) Differentially
865 methylated H3K27me3 between WT and cKO annotated by genomic location using ChIPseeker
866 package, TSS +/- 3000 bp. D) GO Terms and FDR for genes nearest genomic promoters within
867 H3K27me3 Up and Down (due to *Kdm6b*-cKO) peaks. E) Distribution of Log_2Fold Change
868 Expression (WT v cKO, computed using DESeq2) as a function of unchanged, H3K27me3 Up and
869 H3K27me3 Down genomic promoters between WT and cKO (one-way ANOVA, * indicates $p <$
870 0.05). F) Representative genes containing H3K27me3 Up genomic promoter peaks *Grm4* and
871 *Gabbr2* and corresponding RNA-seq tracks between WT and cKO mice (y-axes for ChIP-seq and
872 RNA-seq tracks are autoscaled separately, according to data range in current view).
873

874 **Fig 4. H3K27me3 removal is followed by gain of H3K27me3 and chromatin accessibility at gene**
875 **promoters**
876 A) (Left) Binding Analysis for Regulation of Transcription (BART) for genes near H3K27me3 Down
877 peaks (x-axis) and near all H3K27me3 peaks (y-axis) plotted by -$\log_{10}$p-adj. (Right) Metagene plots
878 for ZIC ChIP-seq signal at genes near all H3K27me3 peaks, genes with H3K27me3 Up and genes
879 with H3K27me3 down. B) (Left) Percentage of genes near H3K27me3 Down promoter peaks that
880 are also ZIC1/2 Up (Log_2Fold Change > 1, P60/P7, ZIC1/2 ChIP-seq). (Right) GO Terms and FDR for
881 genes nearest to H3K27me3 Down promoter peaks that are also ZIC1/2 Up, and not ZIC1/2 Up.
882 C) ZIC ChIP-seq tracks at P7 and P60 at synaptic genes *Grm4* and *Grin2c* (y-axes for ChIP-seq are
883 autoscaled separately, according to data range in current view). D) (Left) Distribution of Log_2Fold
884 Change of H3K27ac enrichment as a function of H3K27me3 Down and H3K27me3 Up described
885 in Fig 2; and (Right) Metagene plots showing H3K27ac ChIP-seq signal at genes with H3K27me3
886 Up and H3K27me3 Down. E) (Left) Distribution of Log_2Fold Change of DNase Hypersensitivity as
887 a function of H3K27me3 Down and H3K27me3 Up described in Fig 2; and (Right) Metagene plots
888 showing DNAse-seq signal at genes with H3K27me3 Up and H3K27me3 Down. F) H3K27ac ChIP-
889 seq and DNAse-seq tracks at P7 and P60 at synaptic gene *Grin2c* (upper), and early gene *Atoh1*
890 (lower) (y-axes for ChIP-seq are autoscaled separately, according to data range in current view).
891
892 **Fig 5. CGN Culture System refines temporal dynamics of H3K27me3 changes at gene promoters**
893 A) Schematic describing CGN culture protocol over 7 days *in vitro* annotated with early and late
894 CGN genes. B) Differentially methylated H3K27me3 CUT&RUN peaks annotated by genomic
895 location, between DIV1-3, 3-5, 5-7 and 1-7 time points. C) Percentage of differential H3K27me3
896 CUT&RUN peaks between DIV1-3, DIV3-5, DIV5-7 and DIV1-7 annotated by genomic region
897 (Annotation performed using ChIPseeker package, TSS +/- 3000 bp). D) (Left) Heatmap of
898 hierarchical clustered VST-transformed DESeq2-normalized counts of differential H3K27me3
899 CUT&RUN promoter peaks from DIV1-7 (Right) Corresponding GO Terms and FDR associated with
900 nearest gene. E) (Left) Metagene plots for H3K27me3 CUT&RUN signal at 'Gain H3K27me3 at
901 DIV7' and 'Lose H3K27me3 at DIV7' clusters. (Right) CUT&RUN tracks for H3K27me3 for (top)
902 early genes *Myc*, and *Atoh1* and (bottom) late genes *Gabrd* and *Grin2c* at DIV1, 3, 5 and 7 (y-axes

903 for CUT&RUN tracks are autoscaled according to data range in current view). F) Violin plot
904 showing the distribution of Log2FC of gene expression measured by RNA-seq between DIV0 and
905 DIV7 CGNs as a function of clustering performed in E (one-way ANOVA, * indicates $p < 0.05$).
906
907 **Fig 6. EZH2 catalytic activity temporally regulates CGN maturation in culture by depositing**
908 **H3K27me3 at early CGN genes**
909 A) (Left) Western blot of acid extracted histones from CGNs treated for H3K27me3 and total
910 Histone H3 (n=3 biological replicates). CGNs were treated with GSK-J4 or GSK-126 at DIV1 and
911 harvested at DIV5, (Right) Quantification of Western Blot. B) MA plot describing differential
912 methylation due to GSK126 treatment in cultured CGNs (FDR < 0.05 and |L2FC| > 1) (n=3
913 biological replicates). C) Metagene plots for H3K27me3 peaks of DMSO and GSK-126 treated
914 CGNs at genes near (Left) All H3K27me3 promoter peaks, (Center) genes that gain H3K27me3 at
915 DIV7, and (Right) genes that lose H3K27me3 at DIV7, described in Fig 5E. D) (Upper) Volcano plot
916 for differentially expressed genes measured by RNA-seq between DMSO and GSK-126 treated
917 CGNs, (Lower) corresponding GO Terms and FDR for up- and downregulated genes. E) (Left)
918 Relationship between gene expression changes during CGN maturation in culture and due to
919 GSK-126 treatment. (Right) Violin plot showing the distribution of Log2FC of gene expression
920 between DMSO and GSK-126 treated CGNs as a function of clustering performed in Fig 5D (one-
921 way ANOVA, * indicates $p < 0.05$. F) (Upper) CUT and RUN tracks and (Lower) RNA-seq tracks for
922 early genes *Ebf3* and synaptic gene *Gabrd*, for DMSO and GSK126 treated CGNs.
923
924
925
926
927

Figure 1. The maturing mouse cerebellum undergoes a genome-wide redistribution of H3K27me3 dominated by loss at promoters

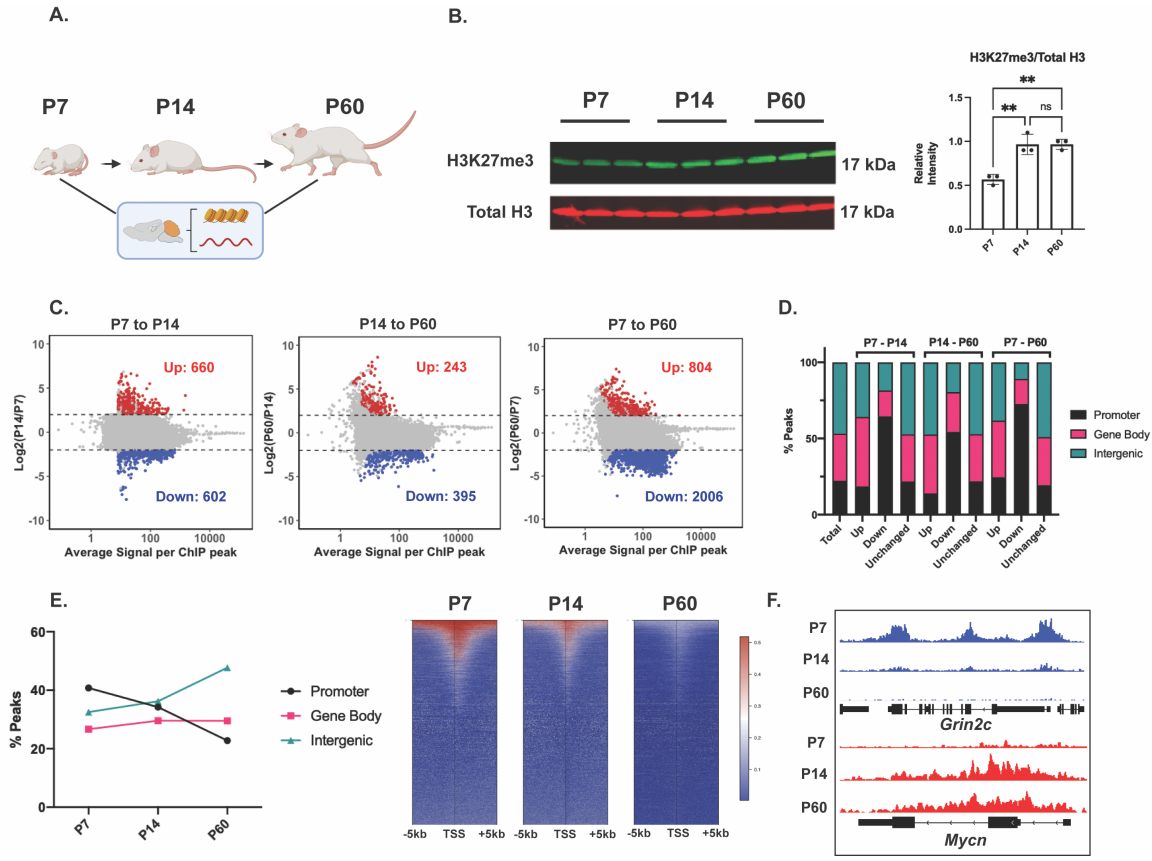

Figure 2. Differentially methylated promoters cluster by turnover kinetics and correlate with CGN maturation gene expression

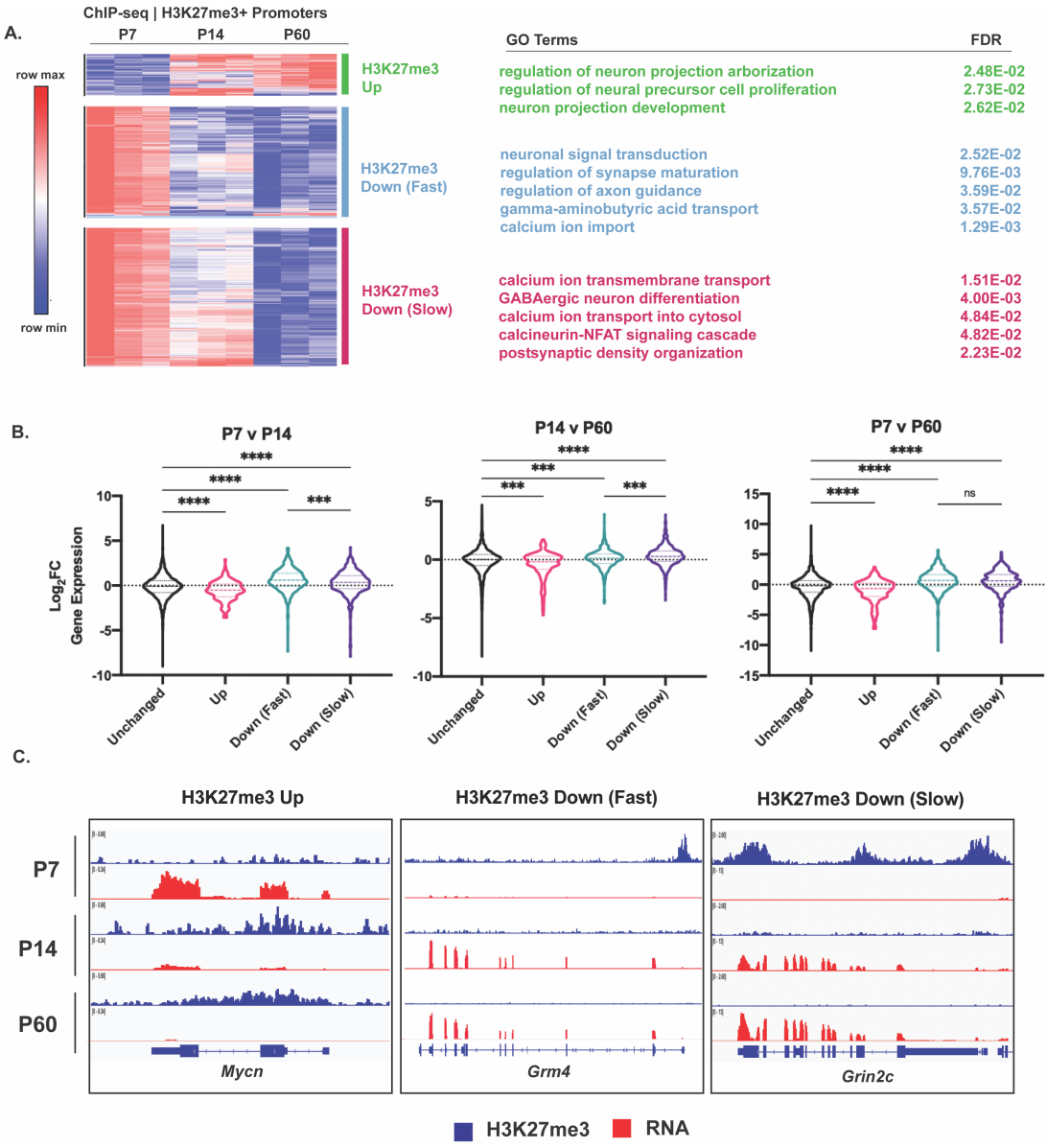

Figure 3. *Kdm6b* knockout in CGN precursors impairs CGN maturation via hypermethylation of CGN maturation gene promoters

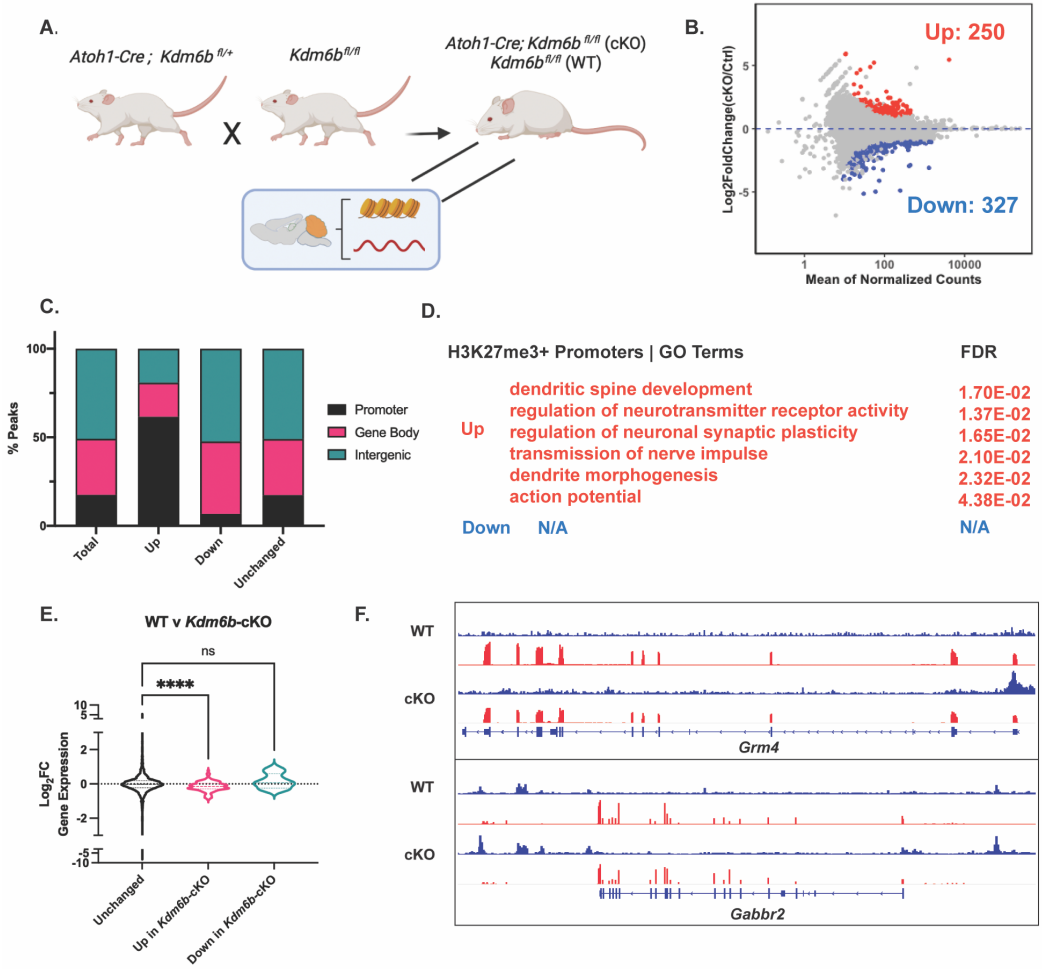

Figure 4. H3K27me3 removal is followed by gain of H3K27me3 and chromatin accessibility at gene promoters

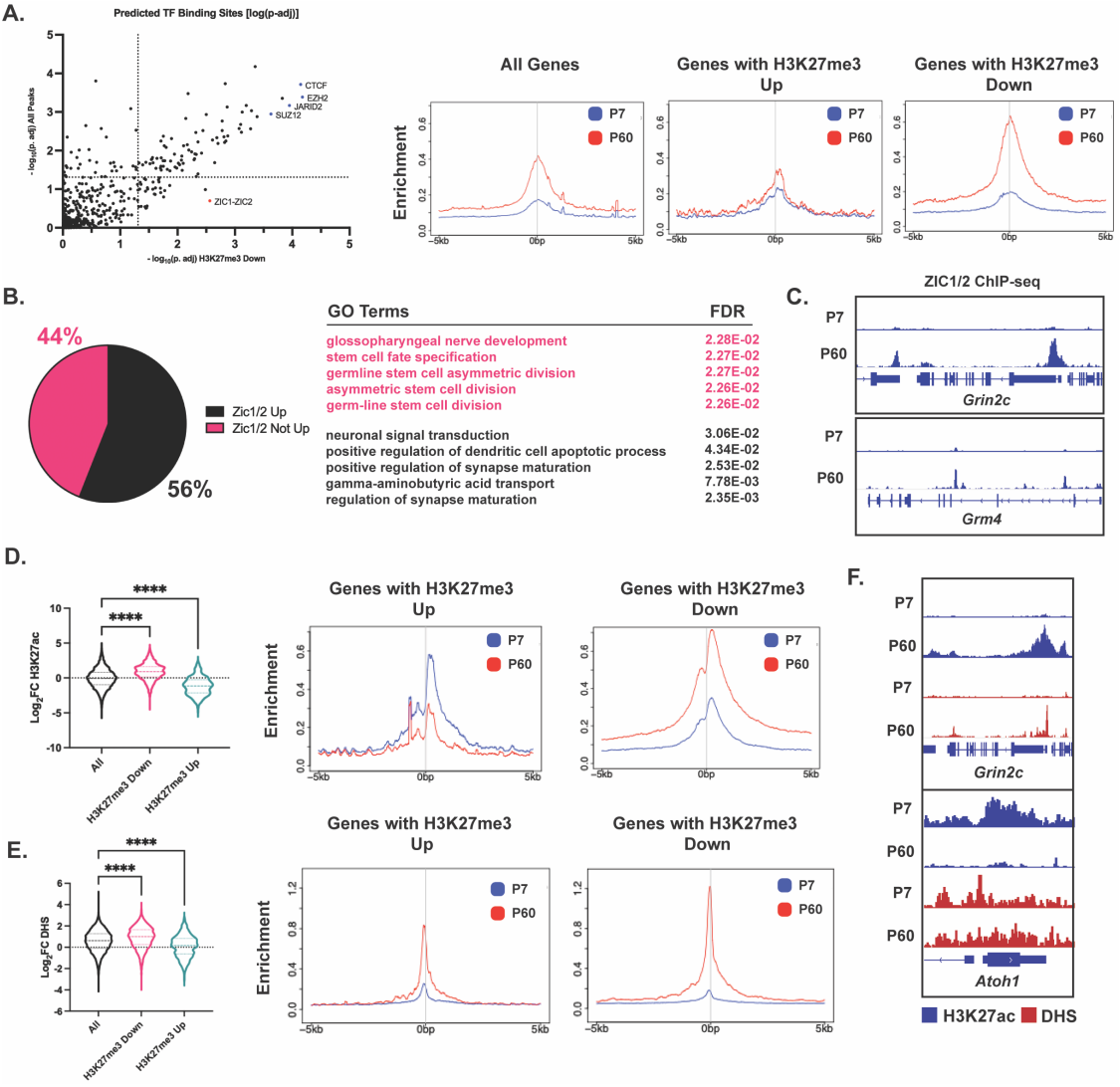

Figure 5. CGN Culture System refines temporal dynamics of H3K27me3 changes at gene promoters

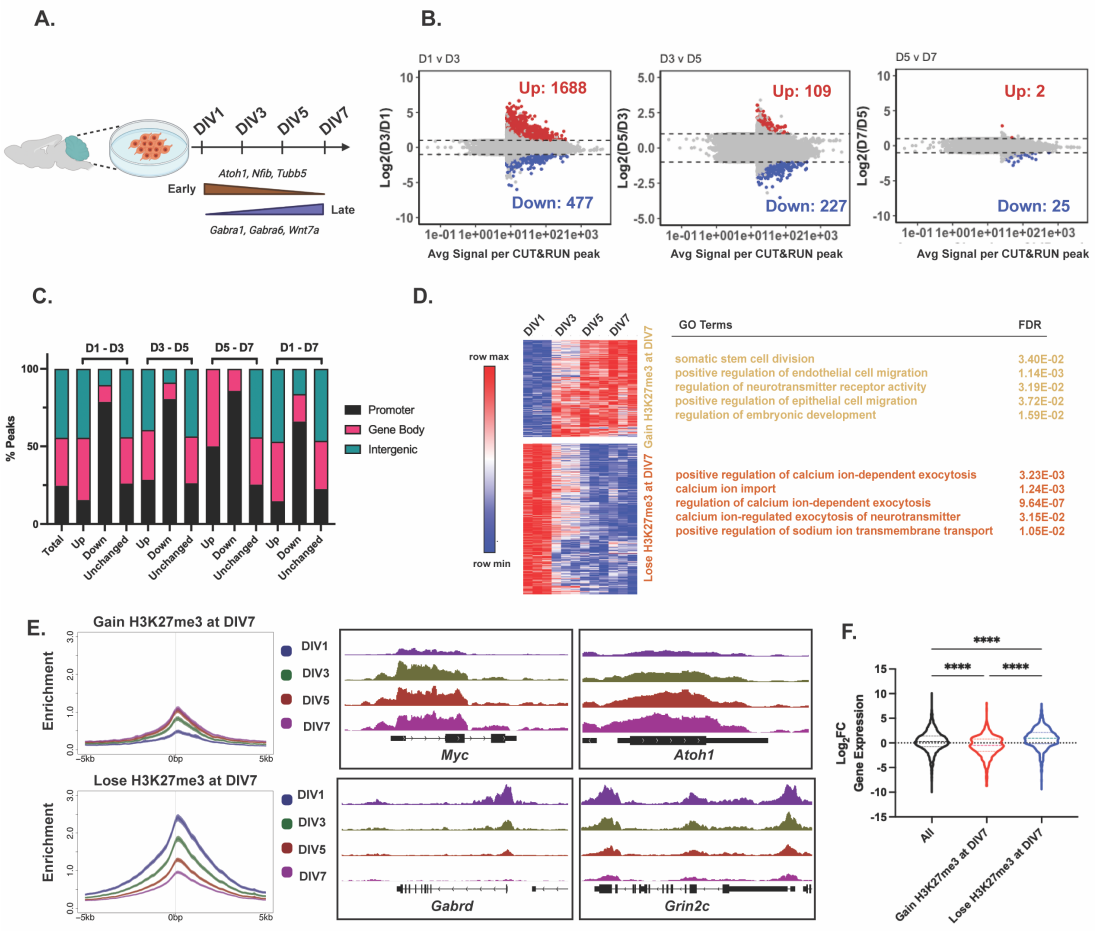

Figure 6. EZH2 catalytic activity temporally regulates CGN maturation in culture by depositing H3K27me3 at early CGN genes

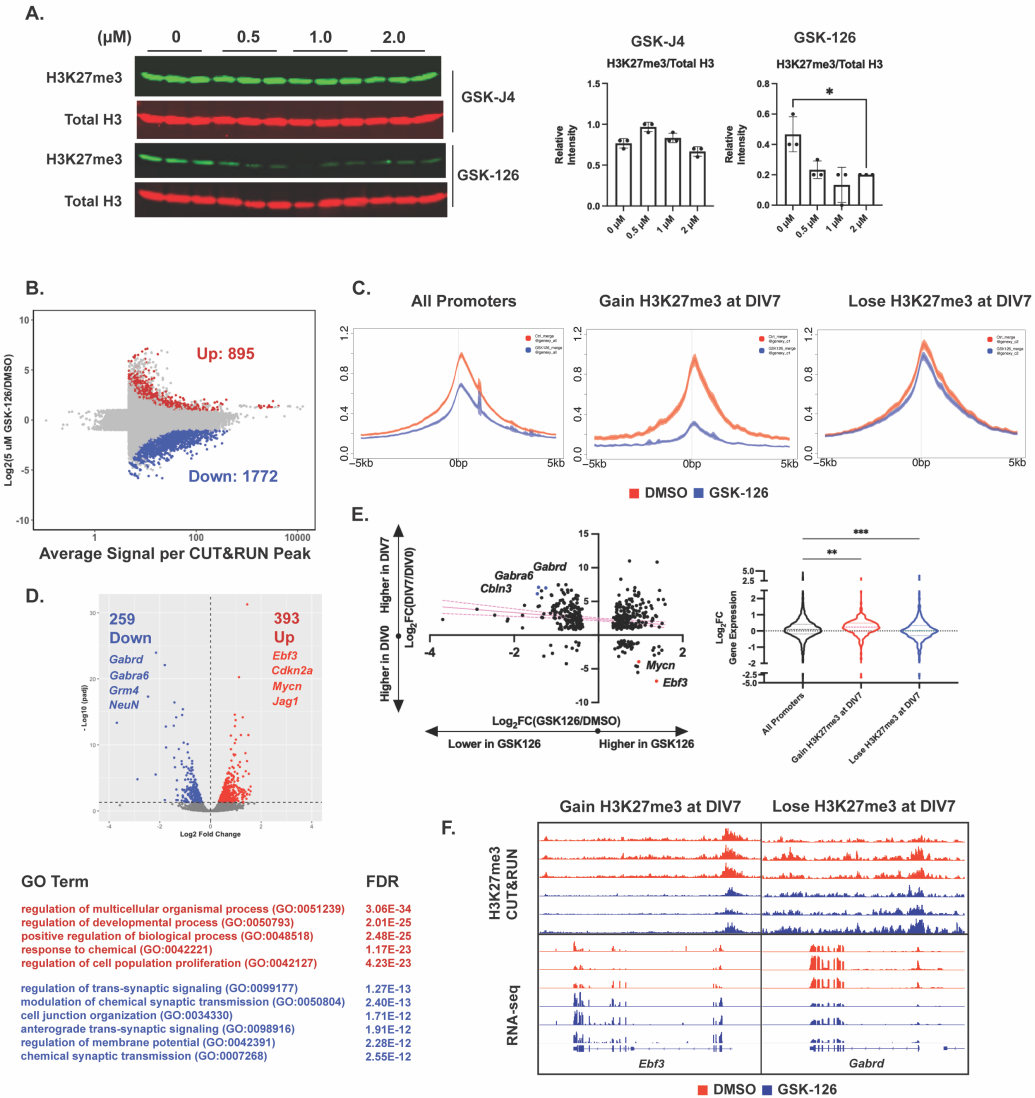

GO Term	FDR
regulation of multicellular organismal process (GO:0051239)	3.06E-34
regulation of developmental process (GO:0050793)	2.01E-25
positive regulation of biological process (GO:0048518)	2.48E-25
response to chemical (GO:0042221)	1.17E-23
regulation of cell population proliferation (GO:0042127)	4.23E-23
regulation of trans-synaptic signaling (GO:0099177)	1.27E-13
modulation of chemical synaptic transmission (GO:0050804)	2.40E-13
cell junction organization (GO:0034330)	1.71E-12
anterograde trans-synaptic signaling (GO:0098916)	1.91E-12
regulation of membrane potential (GO:0042391)	2.28E-12
chemical synaptic transmission (GO:0007268)	2.55E-12